Nano Research

Open Access

Research Article

Supercritical CO_2-enabled dry processing of polymer electrolytes

Qinghuang Lian[1,§], Pengju Liu[1,§] ✉, Wenshu Wang[1,§], Huijin Zhan[1], Yi Xu[1], Chenyang Gu[1], Hongbo Shu[2], Jing Li[2], Huabin Kong[1], Guohua Chen[1], and Hongwei Chen[1] ✉

[1] *College of Materials Science and Engineering, Huaqiao University, Xiamen 361021, China*
[2] *School of Materials and Advanced Manufacturing, Hunan Key Laboratory of Electrochemical Green Metallurgy Technology, Hunan University of Technology, Zhuzhou 412007, China*
§ *Qinghuang Lian, Pengju Liu, and Wenshu Wang contributed equally to this work.*

Cite this article: *Nano Research*, **2026**, *19*, 94908655. https://doi.org/10.26599/NR.2026.94908655

ABSTRACT: The fabrication of polymer-based solid-state electrolytes (SSEs) is often limited by solution-based processing that requires organic solvents and restricts the choice of polymer matrices. Here, we report a solvent-free dry-processing strategy mediated by supercritical CO_2. Leveraging its gas-like diffusivity and liquid-like solvation capability, supercritical CO_2 enables kinetically favored selective diffusion of lithium salts within poly(ethylene oxide) (PEO), initially into amorphous regions followed by gradual permeation into crystalline domains during treatment. This diffusion-driven microstructural evolution leads to a PEO electrolyte with an ionic conductivity of 4.9 × 10^{-4} S·cm^{-1}, nearly four times higher than its solution-cast counterpart. These findings highlight the role of supercritical CO_2 as a mediator of polymer–salt interactions and provide a solvent-free pathway for fabricating polymer electrolytes with tailored crystallinity.

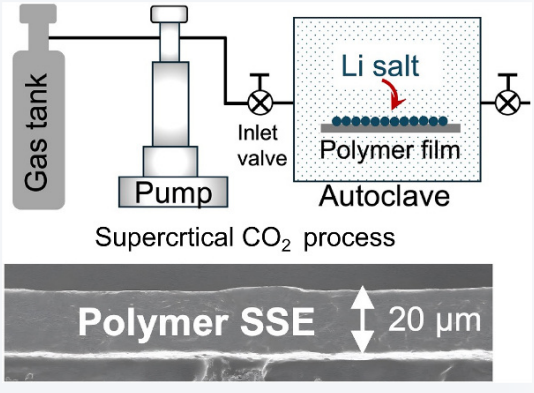

KEYWORDS: solid-state battery, solid-state electrolyte, supercritical CO_2 technology, polymer electrolyte, poly(ethylene oxide) (PEO)

1 Introduction

Solid-state batteries (SSBs), which replace flammable liquid electrolytes with solid-state electrolytes (SSEs), are attracting considerable attention for their intrinsic safety and high energy density [1, 2]. Beyond new materials discovery, processing technologies are equally critical for advancing SSBs. Among them, solution casting mediated by organic solvents has remained the dominant route for fabricating polymer-based SSE membranes [3]. Although solvents assist in forming an ion-conductive network by dissolving Li salts into the polymer matrix, this approach inevitably consumes large amounts of solvent and energy. Consequently, solvent-free dry processing has emerged as a more sustainable alternative [4–6].

In recent years, various dry-processing strategies have been explored, including solvent-free mechanical mixing, melt hot-pressing, and extrusion-based fabrication [7, 8]. These approaches eliminate solvent evaporation steps and shorten processing time, thereby offering advantages in environmental sustainability and potential scalability. However, mechanical mixing often achieves only microscale blending, leading to insufficient salt dispersion within highly crystalline polymer hosts. Melt-processing strategies require polymer softening or melting, which may limit salt incorporation efficiency and are incompatible with insoluble or cross-linked thermoset matrices. As a result, achieving homogeneous salt distribution in polymer electrolytes without solvent assistance remains a significant challenge. However, conventional dry methods based on mechanical mixing achieve only microscale blending, falling short of uniformly dispersing the salt within the polymer host—a prerequisite for efficient ion transport [9–11].

Supercritical CO_2 ($scCO_2$) technology offers a promising route for solvent-free fabrication of polymer SSEs [12]. Operating beyond its critical temperature (31.1 °C) and pressure (7.38 MPa), supercritical CO_2 combines gas-like diffusivity with liquid-like solvation properties (Fig. 1(a)). Unlike wet processing, where polymers and salts co-dissolve and precipitate as the solvent evaporates, the special properties of supercritical CO_2 enable a

Received: January 6, 2026; **Revised:** March 12, 2026
Accepted: March 20, 2026

✉Address correspondence to Hongwei Chen, hwchen@hqu.edu.cn; Pengju Liu, lpengju@hqu.edu.cn

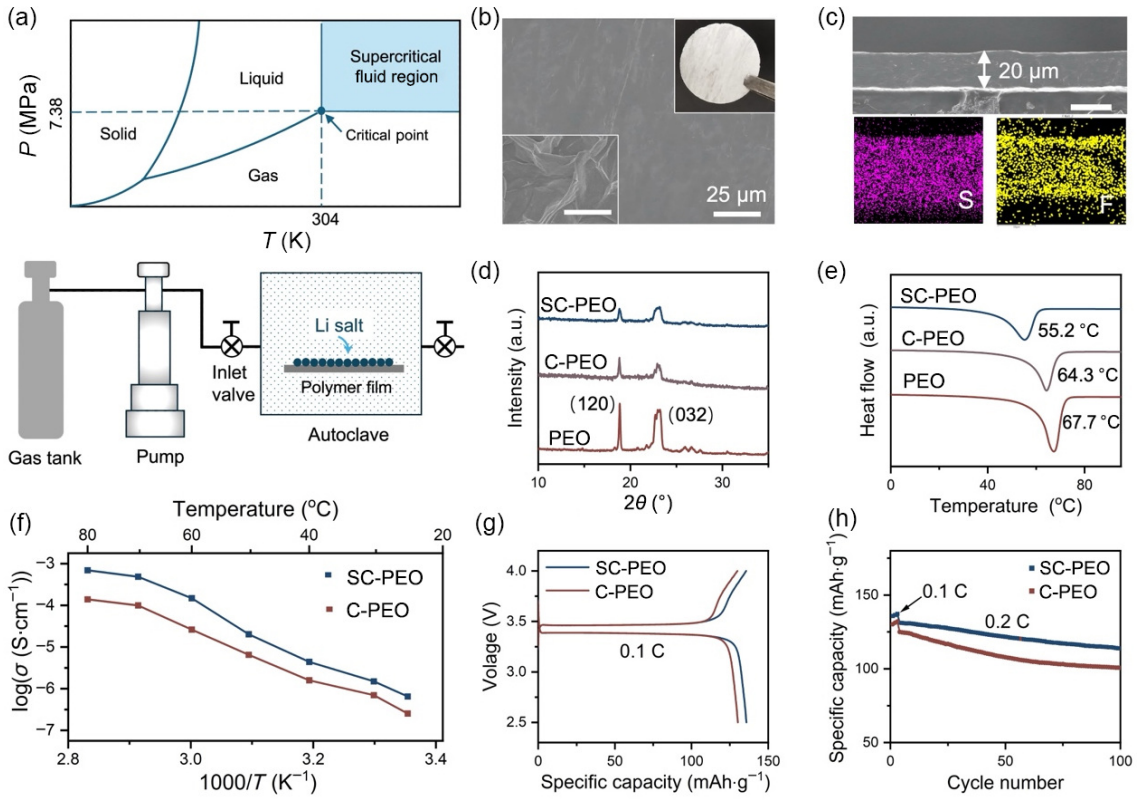

Figure 1 (a) Top: Phase diagram of supercritical CO_2. Bottom: Schematic of electrolyte fabrication using supercritical CO_2. (b) SEM images of SC-PEO: The lower left shows morphology after supercritical CO_2 treatment, displaying irregular undulations; the upper right shows the film after fast hot pressing, and the corresponding SEM image indicates a smoother surface. (c) Cross-sectional view of SC-PEO with corresponding elemental mapping images for S and F. ((d) and (e)) XRD patterns and DSC curves of blank PEO, C-PEO, and SC-PEO samples. (f) Temperature-dependent ionic conductivity of C-PEO and SC-PEO. ((g) and (h)) Charge–discharge curves and cycling performance of solid-state LFP batteries with different electrolytes.

diffusion–permeation process of Li salts within a pre-formed polymer membrane without organic solvents, driven by the high diffusivity and low surface tension of supercritical CO_2 [13]. This approach, which completely eliminates the use of organic solvents, offers several advantages, including lower energy consumption and the recyclability of CO_2 [14].

In this study, we employed supercritical CO_2 technology as a dry fabrication strategy for polymer SSEs, demonstrated using poly(ethylene oxide) (PEO)-based SSE as a proof of concept. Under supercritical CO_2 conditions, the Li salts preferentially permeate the amorphous regions and then gradually diffuse into the crystalline domains. This unique selective diffusion process is fundamentally different from both the simple physical blending process of conventional dry methods and the dissolution–reprecipitation pathway of casting methods. It enables efficient incorporation and uniform spatial distribution of salts into the polymer, without using any organic solvents. The resulting PEO electrolyte achieves an ionic conductivity of 4.9×10^{-4} S·cm^{-1}, nearly four times higher than that of conventional wet-cast membranes. Beyond soluble thermoplastic polymers, we further extend this strategy to insoluble thermoset polymers, exemplified by hydrogenated nitrile butadiene rubber (HNBR). Although the resulting electrolyte exhibits a relatively low ionic conductivity (~ 10^{-6} S·cm^{-1}) at room temperature, it demonstrates the supercritical CO_2-assisted process to incorporate lithium salts into otherwise inaccessible cross-linked polymer matrices. In contrast to conventional applications, our work exploits supercritical CO_2 not merely as a processing medium but as an active mediator of polymer–salt interactions [15, 16]. This distinction highlights the conceptual difference between morphology modification in previous $scCO_2$ studies and the salt incorporation mechanism demonstrated here.

2 Experimental

2.1 PEO film fabrication

The PEO film prepared using the casting technique was labeled as C-PEO and was fabricated as follows. Briefly, 1000 mg of PEO and 130 mg of lithium bis(trifluoromethanesulfonyl)imide (LiTFSI) (with an ethylene oxide to lithium ion (EO:Li) ratio of 50:1) were dissolved in approximately 40 mL of acetonitrile solvent and stirred thoroughly to form a clear solution. This solution was then poured into a polytetrafluoroethylene (PTFE) mold and dried overnight at 80 °C for 12 h under argon and at 80 °C for 12 h under vacuum. The final product was a C-PEO film with a diameter of 12 mm and a thickness of approximately 24 μm.

The PEO film prepared using the supercritical CO_2 technique was labeled as SC-PEO and was fabricated as follows. PEO powder was first hot-pressed into films with a thickness of approximately 24 μm, then punched into disks with a diameter of 12 mm. LiTFSI (with an EO:Li ratio of 50:1) was weighed and evenly spread on the surface of the PEO films. These films were quickly transferred into the reactor, which was sealed and vacuumed to −0.1 MPa. Then CO_2 was introduced, maintaining a temperature of 35 °C and a pressure of 10 MPa. The reaction proceeded for 60 min under these conditions. After that, the pressure was gradually reduced to

atmospheric levels at a rate of approximately 0.05 MPa·min^{-1}. The resulting films were quickly hot-pressed at 50 °C and transferred to a glove box for subsequent testing. Hydrogenated nitrile rubber films were prepared similarly, with a hot-press temperature of approximately 80 °C while keeping the supercritical conditions unchanged.

2.2 Li iron phosphate (LFP) cell preparation

The LFP composite cathodes consisted of 75 wt.% LFP, 10 wt.% Super P, 10 wt.% PEO-LiTFSI (with an EO:Li ratio of 15:1), and 5 wt.% polyvinylidene fluoride (PVDF). After dissolving PEO and PVDF in N-methyl-2-pyrrolidone (NMP), LFP, Super P, and LiTFSI were added, and the mixture was sealed and stirred vigorously overnight. The resulting slurries were cast onto aluminum foil using a doctor blade with a gap of 100 μm. The casting process was followed by drying at 80 °C for 12 h under argon and then at 100 °C for 12 h under vacuum. All operations were performed inside a glove box. The cathodes were punched into disks with a diameter of 12 mm, with a mass loading of approximately 2 mg·cm^{-2}. Li foil was used as the anode. SC-PEO and C-PEO membranes were placed between the cathode and anode, and the components were sealed into CR2032 coin cells. The cells were treated at 70 °C for 12 h before testing. Galvanostatic cycling was conducted using the NEWARE battery test system (NEWARE Technology Ltd., Shenzhen, China) at 50 °C.

3 Results and discussion

3.1 Supercritical technology for polymer SSE fabrication

The supercritical equipment mainly consists of a CO_2 source, a pressurizing pump, and a high-pressure autoclave (Fig. 1(a), bottom). In a typical experiment, the polymer matrix was first hot-pressed into a thin film, evenly sprinkled with Li salt, and then supercritical treated into the autoclave (Fig. S1 in the Electronic Supplementary Material (ESM)). PEO (M_W = 5,000,000 g·mol^{-1}) was chosen as the model polyether due to its wide applications in solid-state Li batteries (SSLBs) [17, 18]. PEO membranes with Li salt (LiTFSI) (with an EO:Li ratio of 50:1) were prepared using both the supercritical method (SC-PEO) and conventional casting method (C-PEO) for comparison.

Scanning electron microscopy (SEM) images confirm that after the supercritical process, the SC-PEO membrane's surface remains largely smooth with some micrometer-scale irregular undulations likely caused by polymer deformation under the supercritical fluid (Fig. 1(b), bottom left; see more in Fig. S2 in the ESM). These irregularities can be easily flattened by subsequent fast hot pressing (Fig. 1(b)). SEM also indicates that the final membrane's cross-section is dense and pore-free (Fig. 1(c)). Corresponding energy dispersive X-ray spectroscopy (EDX) mapping images clearly show the uniform distribution of S and F elements from LiTFSI across the cross-section of SC-PEO, confirming homogeneous distribution of LiTFSI. Fourier transform infrared (FTIR) spectroscopy analysis also confirms the presence of Li salt (Fig. S3 in the ESM). X-ray diffraction (XRD) patterns and differential scanning calorimetry (DSC) curves of SC-PEO and C-PEO indicate that adding LiTFSI to PEO significantly broadens the crystalline diffraction peaks and weakens the melting peaks of the PEO matrix, regardless of the fabrication method (Figs. 1(d) and 1(e)). This can be attributed to the disruption of PEO crystallinity by Li salts, according to conventional understanding [19, 20]. The absence of diffraction peaks for LiTFSI crystals also suggests that LiTFSI is well-dispersed in the PEO matrix through supercritical technology (Fig. S4 in the ESM). Notably, SC-PEO shows a more significant reduction in crystallinity (particularly reflected in the lowered melting point), which may enhance ionic conductivity, as ion diffusion primarily occurs in the amorphous regions of the polymer [21–23]. Indeed, the ionic conductivity of SC-PEO reaches approximately 4.9 × 10^{-4} S·cm^{-1} at 80 °C (Fig. 1(f)), four times higher than that of C-PEO (1.2 × 10^{-4} S·cm^{-1}). Although copolymerization or additive incorporation can enhance PEO's conductivity by 1–2 orders of magnitude [24], we intentionally chose this simple binary system comprising only classic linear PEO and salt for this study, because it enables a clearer investigation of supercritical effects on matrix evolution. Besides, the SC-PEO membrane exhibits slightly increased elongation at break and slightly reduced tensile stress, which may be attributed to the plasticizing effect of CO_2 (Fig. S5 in the ESM) [25].

To assess the applicability in SSLBs, both SC-PEO and C-PEO membranes, with similar thicknesses (~ 24 μm), were used for solid-state LFP cells. Their charge–discharge behaviors are similar, with the SC-PEO cell showing a specific capacity approximately 5 mAh·g^{-1} higher at 0.1 C (Fig. 1(g)). Both SSLBs exhibit similar cycling stability, with typical capacity retention of around 86% and 80% for SC-PEO and C-PEO cells over 100 cycles at 0.2 C (Fig. 1(h) and Fig. S6 in the ESM). These findings highlight supercritical CO_2 technology as a promising alternative to conventional casting methods, with the SC-PEO membrane offering modest yet meaningful improvements in conductivity and cell capacity.

3.2 Thermodynamic and kinetic evolution during supercritical process

Based on previous research in supercritical CO_2-assisted polymer foaming, it is reasonable to propose a process where supercritical CO_2 dissolves LiTFSI and infuses it into the polymer matrix [26]. As pressure is released, the CO_2 exits, leaving LiTFSI uniformly distributed within the matrix. To advance this technology, we need to understand the thermodynamic and kinetic evolution of CO_2 and Li salt dissolution in polymer matrices under supercritical conditions [27].

Thermodynamically, the key to CO_2 dissolution in polymers is improving the interaction between CO_2 and polymer [28, 29]. This interaction can be evaluated by their difference in solubility parameters ($\Delta\delta$, see Note S1 in the ESM). According to traditional polymer theory, the smaller the $\Delta\delta$, the more easily the two materials can dissolve in each other. Greenhalgh et al. found that when $\Delta\delta$ is between 1.6 and 7.5, relatively uniform solid dispersions can be achieved [30]. Simulation results in Fig. 2(a) show that the solubility parameter (δ) of CO_2 is 14.84 (J·cm^{-3})$^{0.5}$ (under 15 MPa, 35 °C), while PEO (with a repeat unit of 6) has a δ of 19.11 (J·cm^{-3})$^{0.5}$, yielding a $\Delta\delta$ of 4.27 (J·cm^{-3})$^{0.5}$. That means CO_2 could dissolve in PEO, consistent with experimental results. Note that CO_2 solubility also depends on the polymer's molecular weight and other factors. Simulations of the polymer chains with repeat units of 6, 10, and 14 reveal that as the repeating units increase, the δ of PEO decreases from 19.11 to 18.94 (J·cm^{-3})$^{0.5}$, indicating that higher molecular weight PEO has a greater ability to dissolve CO_2. That is why we selected moderate PEO with M_w = 5,000,000 g·mol^{-1} in this study.

To further explore the microscopic interaction between polymer chains and CO_2, we simulated a system of eight PEO chains mixed

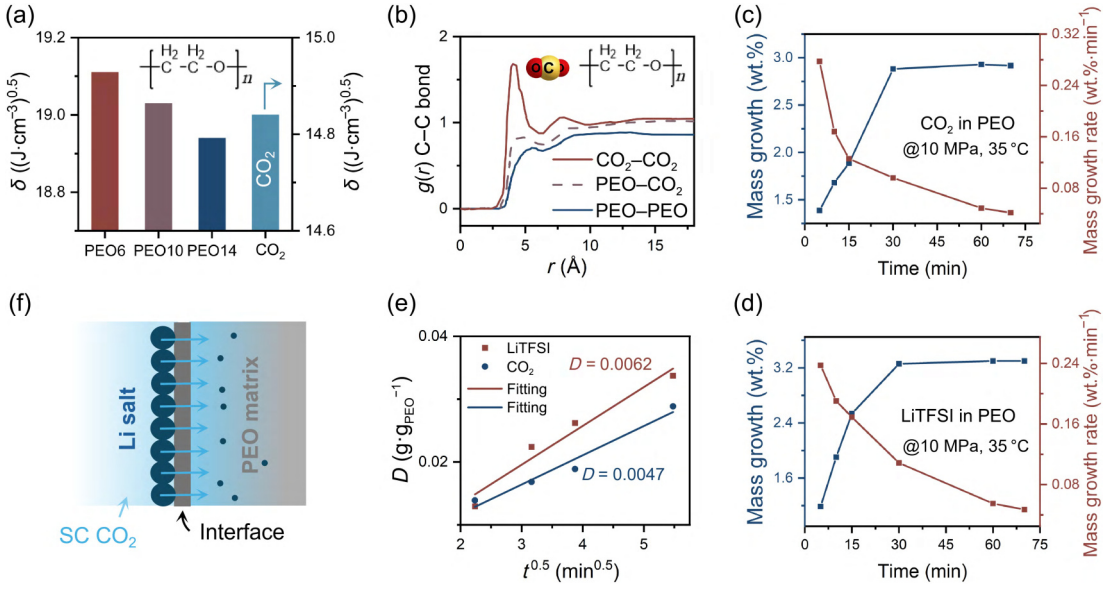

Figure 2 (a) Solubility parameters of CO_2 and PEOs with varying lengths. (b) Radial distribution functions of C–C atomic pairs for CO_2–CO_2, PEO–CO_2, and PEO–PEO interactions. ((c) and (d)) Dissolved mass ratio and dissolution rate of (c) CO_2 and (d) LiTFSI in PEO over time. (e) Corresponding diffusion coefficients of CO_2 and LiTFSI in PEO. (f) Schematic of Li salt diffusion in PEO assisted by supercritical CO_2.

with 1000 CO_2 molecules under supercritical conditions. As shown in Fig. 2(b), the radial distribution function ($g(r)$, where g stands for the radial distribution function value and r stands for the radial distance) of C–C atomic pairs in the PEO–CO_2 system is slightly higher than in PEO–PEO, indicating a preferential approach of CO_2 toward PEO's carbon atoms. However, it should also be noted that the $g(r)$ for PEO–CO_2 is significantly lower than for CO_2–CO_2, suggesting only partial miscibility between PEO and CO_2. These findings align with the solubility parameter calculations and emphasize that the interaction between the polymer and CO_2 is key to CO_2 dissolution.

To enhance ionic conductivity, it is critical to understand the diffusion behavior of CO_2 and Li salts within the PEO matrix from a kinetic perspective. As shown in Fig. 2(c), supercritical CO_2 gradually dissolves into PEO, reaching equilibrium after 0.5–1 h with a final solubility of about 2.9 wt.%. The corresponding dissolution rate indicates that CO_2 initially diffuses rapidly into PEO, and this rate declines over time. LiTFSI follows a similar behavior in PEO, achieving a final solubility of approximately 3.3 wt.% (Fig. 2(d)). The apparent diffusion coefficient (D) in PEO during the early dissolution stage can be estimated based on Figs. 2(c) and 2(d), as shown in Fig. 2(e) (see Note S2 in the ESM), where the slope of the fitted curve represents the D values. Notably, diffusion coefficient of LiTFSI (D_{LiTFSI}) is slightly higher than diffusion coefficient of CO_2 (D_{CO_2}), suggesting a faster initial diffusion rate for LiTFSI. This finding is not entirely understood, as theoretically, CO_2, being a gas, should diffuse more easily through the free volume of PEO by hopping, while LiTFSI, with its larger molecular size and reliance on CO_2 as a carrier, would be expected to diffuse more slowly. We hypothesize that coordination interactions between LiTFSI and PEO chains may enhance LiTFSI diffusion, and it awaits further investigation.

Based on the thermodynamic and kinetic studies above, the results support a mechanism in which LiTFSI adsorbed on the PEO surface gradually diffuses into the PEO matrix under supercritical conditions with the assistance of CO_2 (Fig. 2(f)). In this process, careful consideration should be given to the distribution of LiTFSI and the evolution of PEO crystallinity. This is because typical PEO matrices are polycrystalline, with micron-sized, randomly oriented crystalline domains embedded in amorphous regions (schematically illustrated on the left side of Fig. 4, the initial state), where Li^+ conduction predominantly occurs in amorphous regions [31]. To examine these factors, we used Raman spectroscopy to monitor LiTFSI dissolution in PEO and used polarized optical microscopy (PLM), XRD, and DSC to analyze the evolution of PEO's crystalline morphology. Interestingly, PLM images reveal that during the first 15 min of supercritical treatment, the crystallinity of the PEO matrix remains largely unchanged (Fig. 3(a)), still exhibiting birefringence typical of polymer spherulites. The disruption of crystallinity becomes more pronounced thereafter, with PLM image showing that after 60 min of treatment, PEO spherulites are almost destroyed. Raman spectra show a gradual increase in the $TFSI^-$ characteristic peak at ~ 740 cm^{-1} from the start of supercritical treatment, indicating ongoing LiTFSI diffusion into PEO (Fig. 3(b)) [32]. XRD and DSC analyses show broadening of diffraction peaks and a shift of melting peaks to lower temperatures, also reflecting a significantly weakened PEO crystallinity [20]. As shown in Fig. 3(c), we analyzed changes in XRD full width at half maximum (FWHM) and DSC melting peak shifts over treatment time. Both analyses indicate an initial slow decrease in PEO crystallinity, followed by a significant transition to a more amorphous PEO in the later stages, which aligns with observations from PLM.

These analyses suggest that LiTFSI diffuses selectively. It first diffuses into the amorphous regions of PEO before progressing into the crystalline regions, which leads to a significantly weakened PEO crystallinity in the later stages of supercritical process (Fig. 4). This initial preference for amorphous regions may stem from the larger free volume in these regions, which offers more space and lower diffusion barriers for CO_2 and LiTFSI compared to the ordered and compact crystalline regions [33]. During the subsequent diffusion, two primary forces may drive the subsequent diffusion into crystalline regions. First, CO_2 acts as a plasticizer, as previously demonstrated in polymer-forming studies, thus facilitating LiTFSI incorporation into the crystalline domains [34]. Second, the initial selective diffusion would create a concentration gradient of Li^+ and

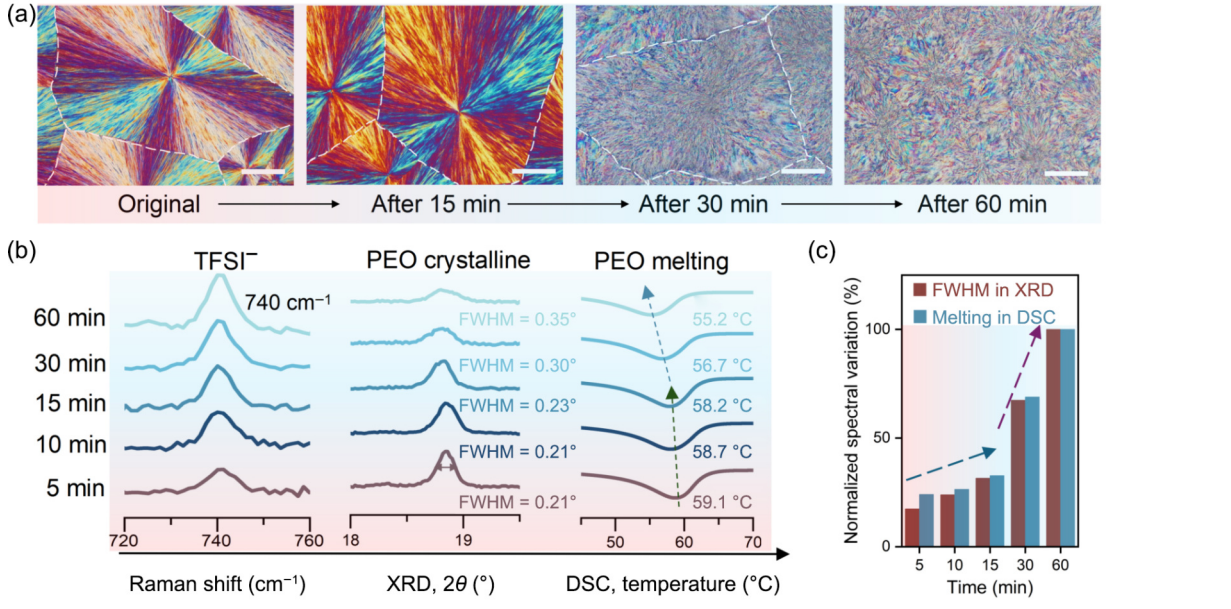

Figure 3 Evolution of the PEO matrix during the supercritical process, analyzed by (a) PLM images and (b) Raman spectra, XRD patterns, and DSC curves. In PLM images, the white dashed lines indicate the boundaries of the PEO spherulites. The scale bar is 50 μm. (c) Corresponding changes in XRD crystalline peak width and DSC melting temperature.

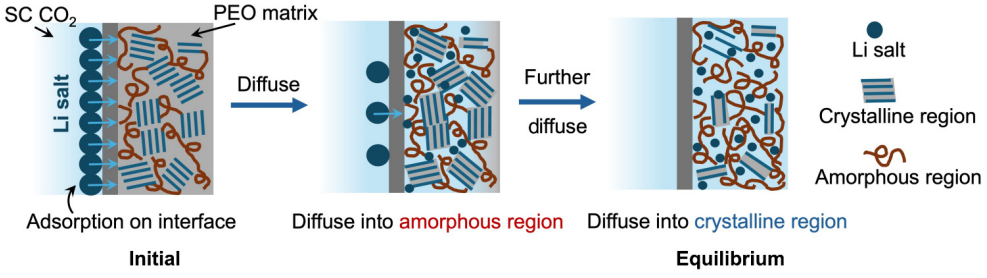

Figure 4 Schematic showing the preferential diffusion of Li salts into amorphous regions of PEO, with subsequent gradual diffusion into crystalline regions.

$TFSI^-$ between the amorphous and crystalline regions, promoting ion migration into the crystalline regions and weakening PEO crystallinity. To test these possible mechanisms, we treated a pure PEO matrix without LiTFSI under the same supercritical conditions. While a slight reduction in crystallinity was observed, the SC-PEO matrix without LiTFSI remained significantly higher in crystallinity than that of LiTFSI-containing PEO (Fig. S7 in the ESM). This suggests that although both driving forces contribute, the concentration gradient is likely playing a more significant role.

Understanding the thermodynamic and kinetic limitations offers guiding principles for optimizing suitable polymer matrices and Li salts for supercritical fabrications. Thermodynamically, the key lies in regulating the $\Delta\delta$ between the polymer matrix, CO_2, and Li salts to enhance their interactions, particularly between CO_2 and the polymer. From a kinetic perspective, besides optimizing supercritical parameters (temperature and pressure) to improve CO_2 solubility, the initial crystallinity of the polymer matrix should be considered [35]. A higher amorphous content may enhance the incorporation and diffusion of CO_2 and thus Li salts, potentially improving the ionic conductivity of electrolytes, though it may compromise mechanical properties [36]. Overall, the supercritical method provides ample opportunities for designing and optimizing polymer SSEs.

3.3 Prospects for supercritical-polymer SSEs

We emphasize that another key advantage of the supercritical approach, unlike traditional casting, is its ability to incorporate Li salts into insoluble and infusible polymer matrices. These polymers, such as cross-linked rubber, possess excellent mechanical properties that combine both softness and strength, making them promising matrix candidates for polymer SSEs [37]. However, their insolubility and infusibility make it difficult to uniformly disperse salts or additives within them. However, supercritical CO_2's unique solubility and diffusivity make it feasible to incorporate salts into the cross-linked polymers. We used cross-linked HNBR as a model matrix and successfully incorporated LiTFSI using the supercritical method (Figs. 5(a) and 5(b)) [38]. The treated rubber, therefore, became an ion conductor with a 2.8×10^{-6} $S \cdot cm^{-1}$ conductivity at 80 °C (Fig. 5(c)). To our knowledge, this is the first successful fabrication of a cross-linked HNBR rubber electrolyte. Although its conductivity remains insufficient for room-temperature operation, this work highlights the potential of supercritical CO_2 to process insoluble polymer electrolytes. Further improvements in ionic transport, through optimization of salt concentration, modification of polymer polarity, or the introduction of mobility-enhancing additives, will be necessary to evaluate the practical applicability of such elastomer-based systems in future studies. Such polymers, previously inaccessible by solution methods, have been largely overlooked despite their chemical tunability and the mechanical advantages of thermosets [39].

This supercritical approach thus offers several advantages over conventional casting: (1) Traditional solvent-based methods rely on

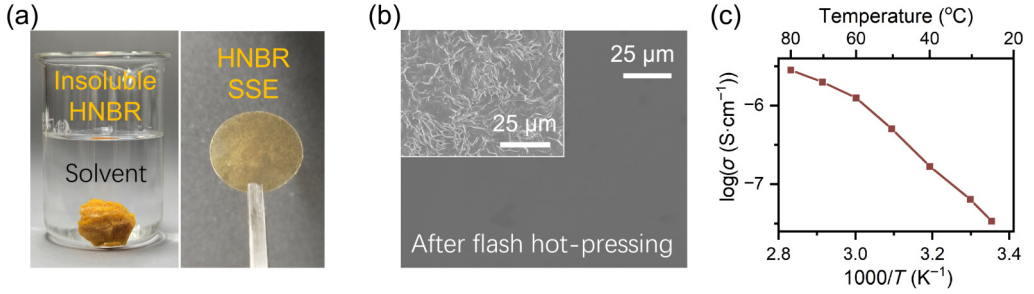

Figure 5 (a) Images of insoluble HNBR and the supercritical CO_2-enabled electrolyte membrane. (b) SEM images of the SC-HNBR surface: Lower left shows morphology after supercritical CO_2 treatment, also displaying irregular undulations. (c) Temperature-dependent conductivity of the HNBR electrolyte.

large volumes of organic solvents, which are costly, difficult to recycle, and environmentally harmful. By contrast, the supercritical technique eliminates the need for these solvents, using only inexpensive, recyclable CO_2. This switch reduces energy consumption and lowers material costs, while significantly reducing the pollution risks associated with solvent recovery (Fig. 5 and supported by the semi-quantitative comparison in Note S3 in the ESM). (2) The supercritical process is also much faster than casting. Without the need for dissolution and lengthy drying steps, supercritical fabrication requires only tens of minutes, compared to the 2–3 days typically needed for solution casting. Given that supercritical equipment is already widely adopted in various industries, this rapid method shows strong potential for electrolyte production. (3) Additionally, as discussed above, the supercritical method uniquely allows the incorporation of Li salts into insoluble and infusible cross-linked polymer matrices, a task that conventional casting methods cannot achieve. This capability significantly broadens the design flexibility for polymer electrolytes, facilitating the development of materials with enhanced mechanical properties and ionic conductivity.

4 Conclusions

In summary, we have successfully employed supercritical CO_2 technology to fabricate two types of polymer electrolytes using PEO and hydrogenated nitrile butadiene rubber as matrices. The PEO electrolyte exhibits a conductivity four times higher than that of conventional casting methods and enables stable cycling in LFP solid-state batteries. Notably, the rubber-based electrolyte—previously unfeasible due to rubber's insolubility and infusibility—was transformed into an effective ionic conductor with a conductivity of 10^{-6} S·cm^{-1}. The supercritical technology provides an environmentally responsible pathway for polymer electrolyte fabrication. By eliminating the need for organic solvents and lowering the process's energy footprint, this approach aligns with sustainability goals, offering a promising avenue for the development of energy storage materials.

Electronic Supplementary Material: Supplementary material (materials, characterization, and theoretical calculation assisted by Materials Studio used in this work; further details of fabrication procedure for polymer electrolytes, surface morphology, FTIR spectra, full XRD spectra, and tensile mechanical test of various PEO; and SEM images, impedance, and cycling stability of the original and cycled cathode) is available in the online version of this article at https://doi.org/10.26599/NR.2026.94908655.

Data availability

All data needed to support the conclusions in the paper are presented in the manuscript and the Electronic Supplementary Material. Additional data related to this paper may be requested from the corresponding author upon request.

Acknowledgements

The authors acknowledge the support from the Natural Science Foundation of Fujian Province (Nos. 2023J02021 and 2024J09038), the National Natural Science Foundation of China (Nos. 22372063, 22302072, and 22302066), the Key R&D Program of Xiamen (No. 3502Z20231059), the Natural Science Foundation of Xiamen (No. 3502Z20227029), and the Significant Science and Technology Project in Xiamen (Future Industry field, No. 3502Z20241033). We acknowledge the support from the Instrumental Analysis Center of Huaqiao University.

Declaration of competing interest

All the contributing authors report no conflict of interests in this work.

Author contribution statement

Q. H. L.: Data curation, formal analysis, writing – original draft. P. J. L.: Conceptualization, funding acquisition, project administration. W. S. W.: Formal analysis, validation. H. J. Z.: Investigation. Y. X.: Validation. C. Y. G.: Investigation. H. B. S.: Investigation. J. L.: Supervision. H. B. K.: Supervision, software. G. H. C.: Supervision. H. W. C.: Funding acquisition, resources, supervision, writing – review & editing. All the authors have approved the final manuscript.

Use of AI statement

None.

References

[1] Chen, R. S.; Li, Q. H.; Yu, X. Q.; Chen, L. Q.; Li, H. Approaching practically accessible solid-state batteries: Stability issues related to solid electrolytes and interfaces. *Chem. Rev.* **2020**, *120*, 6820–6877.

[2] Dai, C.; Stadler, F. J.; Li, Z. M.; Huang, Y. F. E-beam irradiation of poly (vinylidene fluoride-trifluoroethylene) induces high dielectric constant and all-*trans* conformation for highly ionic conductive solid-state electrolytes. *Energy Mater. Dev.* **2023**, *1*, 9370016.

[3] Zhang, X. Y.; Fu, C. K.; Cheng, S. C.; Zhang, C. B.; Zhang, L. C.; Jiang, M.; Wang, J. J.; Ma, Y. L.; Zuo, P. J.; Du, C. Y. et al. Novel PEO-based composite electrolyte for low-temperature all-solid-state lithium metal batteries enabled by interfacial cation-assistance. *Energy Storage Mater.* **2023**, *56*, 121–131.

[4] Yao, W. L.; Chouchane, M.; Li, W. K.; Bai, S.; Liu, Z.; Li, L. T.; Chen, A. X.; Sayahpour, B.; Shimizu, R.; Raghavendran, G. et al. A 5 V-class cobalt-free battery cathode with high loading enabled by dry coating. *Energy Environ. Sci.* **2023**, *16*, 1620–1630.
[5] Schumm, B.; Dupuy, A.; Lux, M.; Girsule, C.; Dörfler, S.; Schmidt, F.; Fiedler, M.; Rosner, M.; Hippauf, F.; Kaskel, S. Dry battery electrode technology: From early concepts to industrial applications. *Adv. Energy Mater.* **2025**, *15*, 2406011.
[6] Yuan, Y.; Chen, L. K.; Li, Y. H.; An, X. F.; Lv, J.; Guo, S. K.; Cheng, X.; Zhao, Y.; Liu, M.; He, Y. B. et al. Functional $LiTaO_3$ filler with tandem conductivity and ferroelectricity for PVDF-based composite solid-state electrolyte. *Energy Mater. Dev.* **2023**, *1*, 9370004.
[7] González, F.; Gregorio, V.; Rubio, A.; Garrido, L.; García, N.; Tiemblo, P. Ionic liquid-based thermoplastic solid electrolytes processed by solvent-free procedures. *Polymers* **2018**, *10*, 124.
[8] Li, Z.; Aboalsaud, A. M.; Liu, X. W.; Thankamony, R. L.; Chen, I. C.; Li, Y. X.; Lai, Z. P. Scalable fabrication of solvent-free composite solid electrolyte by a continuous thermal-extrusion process. *J. Colloid Interface Sci.* **2022**, *628*, 64–71.
[9] Sand, S. C.; Rupp, J. L. M.; Yildiz, B. A critical review on Li-ion transport, chemistry and structure of ceramic-polymer composite electrolytes for solid state batteries. *Chem. Soc. Rev.* **2025**, *54*, 178–200.
[10] Li, Z.; Fu, J. L.; Zhou, X. Y.; Gui, S. W.; Wei, L.; Yang, H.; Li, H.; Guo, X. Ionic conduction in polymer-based solid electrolytes. *Adv. Sci.* **2023**, *10*, 2201718.
[11] Lin, J.; Wu, W. B.; Zhu, J.; Luo, Q.; Wang, L. S.; Mullins, C. B.; Peng, D. L. Unraveling thickness-dependent lithiation behaviors of boride films for all-solid-state thin-film lithium batteries. *Energy Mater. Dev.* **2025**, *3*, 9370062.
[12] Ahn, Y.; Bae, S. J.; Kim, M.; Cho, S. K.; Baik, S.; Lee, J. I.; Cha, J. E. Review of supercritical CO_2 power cycle technology and current status of research and development. *Nucl. Eng. Technol.* **2015**, *47*, 647–661.
[13] Wu, L.; Hou, Z. M.; Luo, Z. F.; Xiong, Y.; Zhang, N. L.; Luo, J. S.; Fang, Y. L.; Chen, Q. J.; Wu, X. N. Numerical simulations of supercritical carbon dioxide fracturing: A review. *J. Rock Mech. Geotech. Eng.* **2023**, *15*, 1895–1910.
[14] Knez, Ž.; Markočič, E.; Leitgeb, M.; Primožič, M.; Hrnčič, M. K.; Škerget, M. Industrial applications of supercritical fluids: A review. *Energy* **2014**, *77*, 235–243.
[15] Yamamoto, Y.; Kawahara, S. Rubbery soft polymer electrolyte membrane with a nanomatrix channel prepared from natural rubber. *ACS Omega* **2025**, *10*, 17576–17583.
[16] Li, Z.; Zhao, Y. N.; Tenhaeff, W. E. 5 V stable nitrile-bearing polymer electrolyte with aliphatic segment as internal plasticizer. *ACS Appl. Energy Mater.* **2019**, *2*, 3264–3273.
[17] Xue, Z. G.; He, D.; Xie, X. L. Poly(ethylene oxide)-based electrolytes for lithium-ion batteries. *J. Mater. Chem. A* **2015**, *3*, 19218–19253.
[18] Su, X.; Xu, X. P.; Ji, Z. Q.; Wu, J.; Ma, F.; Fan, L. Z. Polyethylene oxide-based composite solid electrolytes for lithium batteries: Current progress, low-temperature and high-voltage limitations, and prospects. *Electrochem. Energy Rev.* **2024**, *7*, 2.
[19] Fang, R. Y.; Xu, B. Y.; Grundish, N. S.; Xia, Y.; Li, Y. T.; Lu, C. W.; Liu, Y. J.; Wu, N.; Goodenough, J. B. Li_2S_6-integrated PEO-based polymer electrolytes for all-solid-state lithium-metal batteries. *Angew. Chem., Int. Ed.* **2021**, *60*, 17701–17706.
[20] Appetecchi, G. B.; Henderson, W.; Villano, P.; Berrettoni, M.; Passerini, S. PEO-LiN $(SO_2CF_2CF_3)_2$ polymer electrolytes: I. XRD, DSC, and ionic conductivity characterization. *J. Electrochem. Soc.* **2001**, *148*, A1171–A1178.
[21] Das, D.; Chandrasekaran, A.; Venkatram, S.; Ramprasad, R. Effect of crystallinity on Li adsorption in polyethylene oxide. *Chem. Mater.* **2018**, *30*, 8804–8810.
[22] Sun, W. L.; Zhou, C. J.; Fan, Y. Z.; He, Y. L.; Zhang, H.; Quan, Z. L.; Kong, H. B.; Fu, F.; Qin, J. Q.; Shen, Y. B. et al. Ion co-storage in porous organic frameworks through on-site Coulomb interactions for high energy and power density batteries. *Angew. Chem., Int. Ed.* **2023**, *62*, e202300158.
[23] Sun, W. L.; He, Y. L.; Fang, L.; Zeng, J. R.; Tang, E. L.; Hu, T. P.; Zhang, H.; Lu, D. R.; Hu, C. J.; Quan, Z. L. et al. Refresh organic electrodes for high-power and long-cycle applications. *Nat. Commun.* **2025**, *16*, 5075.
[24] Tan, J. J.; Guo, L. X.; Hu, J. M.; Liu, S. Y. Recent advances in poly (ethylene oxide)-based solid-state electrolytes for lithium-ion batteries. *J. Phys. Chem. C* **2024**, *128*, 17197–17218.
[25] Sauceau, M.; Fages, J.; Common, A.; Nikitine, C.; Rodier, E. New challenges in polymer foaming: A review of extrusion processes assisted by supercritical carbon dioxide. *Prog. Polym. Sci.* **2011**, *36*, 749–766.
[26] Zhai, W. T.; Jiang, J. J.; Park, C. B. A review on physical foaming of thermoplastic and vulcanized elastomers. *Polym. Rev.* **2022**, *62*, 95–141.
[27] Chen, H. W.; Hu, C. J.; Zhang, X. Q.; Chen, L. W. Porous crystalline frameworks as ion-conducting solid-state electrolytes. *Acc. Mater. Res.* **2024**, *5*, 1303–1313.
[28] Jiang, J. J.; Zhou, M. N.; Li, Y. Z.; Chen, B. C.; Tian, F. W.; Zhai, W. T. Cell structure and hardness evolutions of TPU foamed sheets with high hardness via a temperature rising foaming process. *J. Supercrit. Fluids* **2022**, *188*, 105654.
[29] Versteeg, F. G.; de M. R. Lima, G.; Picchioni, F.; Druetta, P. Solubility of supercritical CO_2 in polystyrene. *J. Supercrit. Fluids* **2024**, *213*, 106374.
[30] Greenhalgh, D. J.; Williams, A. C.; Timmins, P.; York, P. Solubility parameters as predictors of miscibility in solid dispersions. *J. Pharm. Sci.* **1999**, *88*, 1182–1190.
[31] Golodnitsky, D.; Strauss, E.; Peled, E.; Greenbaum, S. Review-on order and disorder in polymer electrolytes. *J. Electrochem. Soc.* **2015**, *162*, A2551–A2566.
[32] Yamada, Y.; Furukawa, K.; Sodeyama, K.; Kikuchi, K.; Yaegashi, M.; Tateyama, Y.; Yamada, A. Unusual stability of acetonitrile-based superconcentrated electrolytes for fast-charging lithium-ion batteries. *J. Am. Chem. Soc.* **2014**, *136*, 5039–5046.
[33] Jiang, J. J.; Liu, F.; Yang, X.; Xiong, Z. J.; Liu, H. W.; Xu, D. H.; Zhai, W. T. Evolution of ordered structure of TPU in high-elastic state and their influences on the autoclave foaming of TPU and inter-bead bonding of expanded TPU beads. *Polymer* **2021**, *228*, 123872.
[34] Kikic, I.; Vecchione, F.; Alessi, P.; Cortesi, A.; Eva, F.; Elvassore, N. Polymer plasticization using supercritical carbon dioxide: Experiment and modeling. *Ind. Eng. Chem. Res.* **2003**, *42*, 3022–3029.
[35] Kiran, E.; Sarver, J. A.; Hassler, J. C. Solubility and diffusivity of CO_2 and N_2 in polymers and polymer swelling, glass transition, melting, and crystallization at high pressure: A critical review and perspectives on experimental methods, data, and modeling. *J. Supercrit. Fluids* **2022**, *185*, 105378.
[36] Taki, K.; Kitano, D.; Ohshima, M. Effect of growing crystalline phase on bubble nucleation in poly (l-lactide)/CO_2 batch foaming. *Ind. Eng. Chem. Res.* **2011**, *50*, 3247–3252.
[37] Lee, M. J.; Han, J.; Lee, K.; Lee, Y. J.; Kim, B. G.; Jung, K. N.; Kim, B. J.; Lee, S. W. Elastomeric electrolytes for high-energy solid-state lithium batteries. *Nature* **2022**, *601*, 217–222.
[38] Verdier, N.; El Khakani, S.; Lepage, D.; Prébé, A.; Aymé-Perrot, D.; Dollé, M.; Rochefort, D. Polyacrylonitrile-based rubber (HNBR) as a new potential elastomeric binder for lithium-ion battery electrodes. *J. Power Sources* **2019**, *440*, 227111.
[39] Mindemark, J.; Lacey, M. J.; Bowden, T.; Brandell, D. Beyond PEO—Alternative host materials for Li^+-conducting solid polymer electrolytes. *Prog. Polym. Sci.* **2018**, *81*, 114–143.